

Galaxy Number Counts and Implications for Strong Lensing

C. D. Fassnacht,¹ L. V. E. Koopmans,² and K.C. Wong^{1,3}

¹*Department of Physics, University of California Davis, 1 Shields Avenue, Davis, CA 95616, USA*

²*Kapteyn Astronomical Institute, P.O. Box 800, 9700 AV Groningen, Netherlands*

³*Current Address: Astronomy Department/Steward Observatory, University of Arizona, 933 N. Cherry Ave., Tucson, AZ 85721, USA*

22 February 2024

ABSTRACT

We compare galaxy number counts in Advanced Camera for Surveys (ACS) fields containing moderate-redshift ($0.2 < z < 1.0$) strong gravitational lenses with those in two control samples: (1) the first square degree of the COSMOS survey, comprising 259 ACS fields and (2) 20 “pure parallel” fields randomly located on the sky. Through a Bayesian analysis we determine the expectation values (μ_0) and confidence levels of the underlying number counts for a range of apertures and magnitude bins. Our analysis has produced the following results: (i) We infer that our control samples are not consistent, with the number counts in the COSMOS sample being significantly higher than in the pure parallel sample for $21 \leq F814W \leq 23$. This result matches those found in previous analyses of COSMOS data using different techniques. (ii) We find that small-size apertures, centered on strong lenses, are overdense compared with randomly placed apertures in the control samples, even compared to the COSMOS sample. Correcting for the local clustering of elliptical galaxies, based on the average two-point correlation function reduces this overdensity to the $1-2-\sigma$ level. Thus, the overdensity of galaxies seen along a typical line of sight to a lens can be explained mostly by the natural clustering of galaxies, rather than being due to lenses lying along otherwise biased lines of sight. However, a larger sample of lenses is needed to see if the remaining bias persists when the lens-field uncertainties are smaller. (iii) There is considerable scatter in the lines of sight to *individual* lens systems, but quantities that are linearly dependent on the external convergence (e.g., H_0) should become unbiased if the extra galaxies that cause the bias can be accounted for in the lens models either through direct modeling or via an informed prior on the external convergence. The number counts can be used to set such an informed prior.

Key words: gravitational lensing – large-scale structure of Universe – distance scale

1 INTRODUCTION

Strong gravitational lenses, where multiple images of the background object are formed, are powerful probes of the distribution of mass in the Universe. The properties of the lensed images are, in principle, sensitive only to the projected mass of the lensing object, with no requirements that the mass be luminous or baryonic (e.g., Schneider, Kochanek, & Wambsganss 2006). Most of the lensing signal comes from the primary lensing object – typically a massive early-type galaxy – and, if the lensing object is a member of a galaxy cluster or group, its immediate environment.

However, the distribution of large-scale structure (LSS) along the line of sight to the lens system adds perturbations to the lensing properties. For example, simulations have shown that a non-negligible fraction of lenses can only be produced by having multiple lens planes along the line of sight (Wambsganss, Bode, & Ostriker 2005; Hilbert et al. 2007, 2008). Furthermore, the differences in light travel times along the rays that form the multiple lensed images in a given system can be affected at the level of a few percent (e.g., Seljak 1994) or up to $\sim 10\%$ (e.g.,

Bar-Kana 1996) by the distribution of LSS along that particular line of sight. These effects should be random for random lines of sight, so it should be possible to reduce the LSS uncertainties and exploit the power of gravitational lenses as cosmological tools by averaging over many systems. If, however, lenses lie along biased lines of sight, this reduction will not occur and global parameters such as H_0 determined from large lens samples will be biased.

To date, most observational investigations of the effects of the environment on strong lensing have focused on the local neighborhood of the lens by searching for spectroscopic evidence of galaxy groups and clusters that are physically associated with the lensing galaxy (e.g., Kundić et al. 1997a,b; Fassnacht & Lubin 2002; Momcheva et al. 2006; Fassnacht et al. 2006b; Auger et al. 2007, 2008). Some of these investigations (e.g., Fassnacht & Lubin 2002; Momcheva et al. 2006; Fassnacht et al. 2006b; Auger et al. 2007) have also found mass concentrations along the line of sight that are at different redshifts than the lensing galaxy. However, due to the limitations imposed by requiring spectroscopic redshifts for their analyses, the spectroscopic surveys are necessarily incomplete samples of the line of sight. Most also are also biased be-

cause they preferentially target galaxies expected to be at the redshift of the primary lens. There have also been photometric studies of lens fields in order to evaluate lens environments. These photometric investigations are the closest in concept to the analysis in this paper. However, they focused on either group finding via detection of red sequences or spatial overdensities (Williams et al. 2006; Faure et al. 2004), or on describing the immediate environment of the lensing galaxy by using galaxy colors to strongly favor galaxies likely to be at the redshift of the lens (Auger 2008; Treu et al. 2009). The Auger (2008) work also evaluates the contributions by galaxies along the full line of sight, and so has a component that is very similar to the work presented in this paper. However, it focuses strictly on low redshift lenses ($z \sim 0.1 - 0.3$), while we study a higher redshift sample ($0.2 < z < 1.0$).

In this paper, we investigate the question of whether lens lines of sight are biased by comparing, through Bayesian and frequentist statistics, the number counts of galaxies in fields containing gravitational lenses with those obtained from two control samples. The control samples are chosen to provide reasonable approximations to typical lines of sight through the Universe. All images were obtained with the Advanced Camera for Surveys (ACS; Ford et al. 1998, 2003) aboard the *Hubble Space Telescope* (HST). The underlying idea is that lines of sight that are overdense in galaxies are also overdense in mass, if the underlying redshift distributions are roughly the same. Hence by simply counting galaxies, one can make conservative statements about the lines of sight towards lens galaxies that are not highly model-dependent. We discuss the sample selection and image processing in §2, do a frequentist analysis of the samples in §3, develop and use a Bayesian framework for comparing the samples in §4, briefly describe the number counts for individual lens systems (as opposed to sample averages) in §5, and interpret the results in §6.

2 DATA REDUCTION

In this section we briefly describe the data reduction and catalogue extraction.

2.1 Sample Definition and Data Processing

The lens sample comprises 18 systems which were observed with ACS as part of the CfA-Arizona Space Telescope Lens Survey (CASTLES; GO-9744; PI Kochanek). This sample was defined by taking the full list of lenses observed with ACS as part of the CASTLES program (24 galaxies in all) and only including systems that (1) had total exposure times $\gtrsim 2000$ s, (2) had no extremely bright stars in the field, and (3) had galactic latitudes of $|b| > 10$. Each system was observed through the F555W and F814W filters, but for comparison with the control data sets, we only consider the F814W data. The typical total exposure times through the F814W filter were ~ 2000 – 3000 sec. Details of the observations are given in Table 1. The pipeline-processed data were obtained from the Multi-mission Archive at Space Telescope, and the individual exposures were combined using the *multidriz* package (Koekemoer et al. 2002). We also included in the lens sample deep ACS images of B0218+357 (GO-9450; PI N. Jackson) and B1608+656 (GO-10158; PI Fassnacht), with total F814W exposure times of 48,720 and 28,144 sec, respectively. For easier comparison with the rest of the lens sample we only used the data from the first four F814W exposures on the B1608+656 field, with a combined integration time of 2528 sec.

Table 1. Lens Sample

Lens System	t_{exp} (sec)	z_{lens}	References
JVAS B0218+357	48720	0.685	1,2
CLASS B0445+128	5228	0.557	3,4
CLASS B0850+054	2296	0.59	4,5
CLASS B1608+656	2528	0.630	6
CLASS B2108+213	2304	0.365	7,8
CFRS 03.1077	2296	0.938	9
HE 0435-1223	1445	0.454	10,11
HE 1113-0641	1317	0.75 ^a	12
J0743+1553	2300	0.19	13
J0816+5003	2440	...	14
J1004+1229	2296	0.95	15
RX J1131-1231	1980	0.295	16
SDSS 0246-0825	2288	0.723	17,18
SDSS 0903+5028	2444	0.388	19
SDSS 0924+0219	1148	0.39	20,21
SDSS 1004+4112	2025	0.68	22,23
SDSS 1138+0314	2296	0.445	24
SDSS 1155+6346	1788	0.176	25
SDSS 1226-0006	2296	0.517	24
WFI 2033-4723	2085	0.661	26,24

Redshifts marked with an ^a are photometric redshifts. All other redshifts are spectroscopic.

References: [1] Patnaik et al. (1993), [2] Browne et al. (1993), [3] Argo et al. (2003), [4] McKean et al. (2004), [5] Biggs et al. (2003), [6] Myers et al. (1995), [7] McKean et al. (2005), [8] McKean et al. (2010), [9] Crampton et al. (2002), [10] Wisotzki et al. (2002), [11] Morgan et al. (2005), [12] Blackburne, Wisotzki, & Schechter (2008), [13] Haarsma et al. (2005), [14] Lehár et al. (2001), [15] Lacy et al. (2002), [16] Sluse et al. (2003), [17] Inada et al. (2005), [18] Eigenbrod, Courbin, & Meylan (2007), [19] Johnston et al. (2003), [20] Inada et al. (2003), [21] Eigenbrod et al. (2006a), [22] Inada et al. (2003), [23] Oguri et al. (2004), [24] Eigenbrod et al. (2006b), [25] Pindor et al. (2004), [26] Morgan et al. (2004).

The lens galaxies are at moderate redshifts, with a mean and RMS of $\mu_z = 0.55$ and $\sigma_z = 0.22$, respectively. This should be compared to the environmental investigations of Auger (2008) and Treu et al. (2009), which analyzed the lower redshift SLACS ($z \lesssim 0.3$) sample (e.g., Bolton et al. 2008, 2006). The lens galaxies can be further distinguished from the SLACS lenses in that nearly all of them (17/20) are lensing active galactic nuclei (AGN) rather than galaxies, and all but one of them were selected by targeting the lensed source population rather than targeting the likely lenses as was done in SLACS. Most lens systems with existing time delays have lens redshifts at $z > 0.3$. Thus, this sample, with $z_{lens} \sim 0.5$, and lensed sources that are expected to be variable, is more likely to be representative of lens systems for which time delays, and thus quantities such as H_0 , can be measured.

2.2 Control fields

The first control sample consists of data obtained by the Cosmic Evolution Survey team (COSMOS; Scoville et al. 2007a,b). The COSMOS data consist of a mosaic of approximately two square degrees, with all of the images obtained through the F814W filter. They were obtained as part of a 510-orbit HST Treasury proposal in Cycles 12 and 13 (GO-9822; PI Scoville). Each field has a total exposure time of 2028 sec, comparable in depth to the lens fields. The data have been fully reduced by the COSMOS team (Koekemoer et al. 2007), so it was not necessary to run *multidriz*.

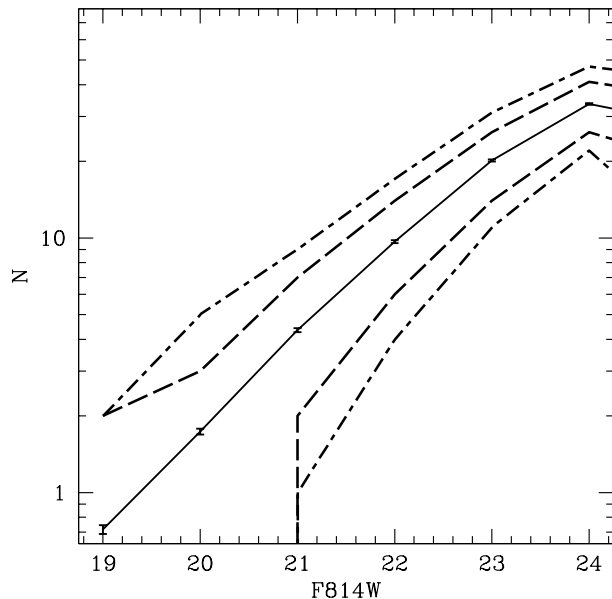


Figure 1. Number counts in the COSMOS fields, using apertures of radius $45''$. There are four such apertures per COSMOS ACS field. The thick solid line represents the mean number counts in each bin, while the negligible error bars on the line show the formal error on the mean. The dashed and dot-dashed lines enclose 68% and 90% of the data, respectively.

zle. Instead the 257 processed science and weight images from Cycle 12 – comprising ~ 1 square degree – were obtained from the COSMOS ACS website hosted by the NASA/IPAC Infrared Science Archive¹.

The second control sample consists of data obtained as part of a pure parallel program to search random fields for emission line galaxies (GO-9468; PI L. Yan). This program included 28 pointings in the F814W filter, of which we used the 20 that successfully passed all of the criteria required for our image processing (hereafter referred to as the “pure parallel fields”). These pure parallel fields cover a total area of ~ 0.06 square degrees. Although the number of pointings is much smaller than obtained with the COSMOS program, the pure parallel fields have the advantage of not being contiguous on the sky and, thus, provide an important check that the COSMOS data do not have some overall bias in the number counts due to sample variance. These data were processed by the a modified version of the pipeline developed as part of the HST Archive Galaxy Gravitational Lens Survey (Marshall et al., in prep) which is designed to produce final images aligned sufficiently well to conduct weak lensing analyses. The modification to the pipeline for the pure parallel fields was simply to change the output pixel scale from the HAGGLES standard $0''.03 \text{ pix}^{-1}$ to $0''.05 \text{ pix}^{-1}$, in order to match the COSMOS pixel scale.

2.3 Object Detection and Flagging

Object catalogs were obtained by running SExtractor (Bertin & Arnouts 1996) on each ACS image. For both the lens-field and control files, the weight maps produced by *multidrizzle* were used to improve the object detection. The magnitudes

used in this paper for all three samples are Vega-based $F814W$ magnitudes measured within the “AUTO” aperture computed by SExtractor. Hereafter, we will use m to designate these $F814W$ Vega magnitudes. We edited the initial catalogs to reject stars and artifacts. Because the *HST* point spread function is simply the diffraction limit of the telescope rather than depending on variable seeing, a simple star-galaxy separation can be achieved by plotting the SExtractor full width at half-maximum (FWHM) parameter versus object magnitude. The stars stand out as a narrow locus of objects all with approximately the same FWHM, up until the point where they saturate (at $m \lesssim 18 - 18.5$). For brighter stars, the locus moves to larger values of the FWHM while still remaining relatively narrow, making it easy to reject the stars. However, this star-galaxy separation method does not catch false detections due to stellar diffraction spikes and bleeding from saturated regions. Most of these objects can be still be flagged automatically because they are often highly elongated. Thus, to select real galaxies from the catalogs, we rejected all sources with: (1) $\text{FWHM} < 0''.13$, (2) $m < 18.5$, and (3) $(b/a) < 0.12$, where a and b are the semimajor and semiminor axes, respectively.

The COSMOS catalogs required additional flagging because the images obtained from the COSMOS ACS science archive contain bands several pixels wide along their left and right edges where cosmic rays are not properly cleaned. Simple spatial masks were sufficient to eliminate the spurious sources associated with the cosmic rays. The COSMOS images were obtained at two fixed roll angles, separated by 180° (e.g., Koekemoer et al. 2007), so that two sets of masking regions were required to flag the resulting catalogs.

2.4 Definition of apertures

We compute galaxy number counts in a set of apertures with radii of $45''/(\sqrt{2})^i$, where $i = 0, 1, 2, 3$. These aperture sizes are chosen to probe how localized any differences between the lens fields and control fields may be. The lens targets are centered on one of the ACS chips, and the $i = 0$ aperture is roughly the largest that can fit on the chip without extending over the chip gap. For apertures with $i > 3$, the numbers of galaxies detected in the apertures start to drop to unacceptably small numbers on the bright end of the luminosity functions. In the case of the lens fields, the apertures are always centered on the lensing galaxy, while for the control fields the apertures were laid down on regular grids to maximize the number of independent apertures on each field while also avoiding the chip edges and chip gap. These grids consist of 4, 9, 16, and 36 apertures per pointing for aperture radii of $45''$, $31''.8$, $22''.5$, and $15''.9$, respectively. Thus, for each choice of aperture size there will always be 20 lens apertures, whereas the number of control field apertures will depend on the aperture size. There will be $(257 \times n)$ COSMOS and $(20 \times n)$ pure parallel apertures, where n represents the aperture-dependent number of grid points per pointing listed above.

Figure 1 shows, as an illustration, the distribution of galaxy number counts in the COSMOS fields inside apertures of radius $45''$, with lines marking the mean number counts and the regions enclosing 68% and 90% of the data. The formal errors on the mean are very small (nearly invisible on the plot), but small number statistics significantly broaden the width of the distribution at the bright end. Furthermore, the 2000 s exposure time for each COSMOS field leads to a turnover of the number counts past $m = 24$. Thus, in the following analysis we only consider objects with $19 \leq m \leq 24$.

Of course, having the lens-field apertures chosen to be cen-

¹ http://irsa.ipac.caltech.edu/data/COSMOS/images/acs_v1.2/

Table 2. KS Test Results

r (")	m	$\log_{10} P_{KS}$		
		Lens–COSMOS	PP–COSMOS	Lens–PP
45.0	19	-0.54	-0.00	-0.40
	20	-2.37	-0.24	-1.89
	21	-0.84	-0.95	-0.63
	22	-0.66	-3.22	-0.49
	23	-0.07	-3.78	-0.03
31.8	24	-0.81	-0.50	-0.61
	19	-0.52	-0.00	-0.45
	20	-1.93	-0.12	-1.73
	21	-0.94	-1.69	-0.83
	22	-0.11	-8.77	-0.08
22.5	23	-0.03	-5.60	-0.02
	24	-0.60	-2.04	-0.52
	19	-0.09	-0.00	-0.07
	20	-0.97	-0.00	-0.90
	21	-1.23	-1.23	-1.15
15.9	22	-0.44	-5.64	-0.40
	23	-0.03	-1.53	-0.02
	24	-0.50	-0.06	-0.46
	19	-0.03	-0.00	-0.03
	20	-0.23	-0.00	-0.22
	21	-0.90	-2.83	-0.87
	22	-0.60	-8.18	-0.58
	23	-0.30	-6.43	-0.29
	24	-0.13	-5.28	-0.13

Results from Kolmogorov–Smirnov tests comparing pairs of samples. Values are the logarithms of the probabilities that the given pair of samples could have produced the observed D values by chance if they were drawn from the same distribution. The “PP” designation refers to the pure parallel sample. Numbers in bold are those with probabilities lower than 0.01.

tered on the lens system introduces two sources of bias. The first is that the lens system itself, consisting of the lensing galaxy and the multiple lensed images of the background source, contributes to the number counts in the aperture. The second bias is that lensing galaxies tend to be massive early-type galaxies and, as such, can be expected to be found in locally overdense environments (e.g., Dressler 1980; Zabludoff & Mulchaey 1998). We control the first bias by flagging the lensing galaxy and all lensed images by hand in the input catalogs. Furthermore, we exclude any galaxies within $\theta = 2''.5$ of the lens systems to avoid any strong magnification biases associated with these bright galaxies, although this is not expected to be a large effect. For typical galaxy-mass lenses, the Einstein ring radii of $\theta_{E_{in}} \sim 1''$ imply that the magnifications of lensed images at $\theta = 2''.5$ are ~ 0.5 magnitude, and the magnification falls off as $\sim 1/\theta$. Therefore, only a small solid angle around each lens produces magnification at this level, suggesting that the number of faint galaxies that are mistakenly placed into a brighter magnitude bin will be minimal. The correction for the second effect is discussed in §4.4. There may be some additional bias in the number counts in the lens fields due to clustering associated with the lensed background object (e.g., Fassnacht et al. 2006a), which for these systems is almost always a massive galaxy hosting an active nucleus. However, we expect this bias in the counts to appear only in the fainter magnitude bins and to be (1) mostly washed out by the large number of faint galaxies along these lines of sight and/or (2) fainter than our $m = 24$ cutoff.

3 FREQUENTIST ANALYSIS

In order to do an initial comparison of the three samples, we use Kolmogorov–Smirnov (KS) tests on three different pairs of samples: lens vs. COSMOS, pure-parallel vs. COSMOS, and lens vs. pure-parallel. These tests are conducted for each combination of aperture size and magnitude. Figure 2 shows examples of cumulative distributions for several combinations of aperture size and magnitude bin. These plots can be used to estimate the KS D value for representative pairs of samples, as well as the sample medians. The results of the KS tests are given in Table 2, and reveal that for most of the aperture–magnitude pairs the lens fields are consistent, at greater than the 10% confidence level, with being drawn from the same distribution as the control fields; only for the comparison to the COSMOS sample in the $m = 20$ bin and the $45''$ aperture is the probability that the two samples are drawn from the same distribution less than 1%. However, the significance of any differences between the lens fields and the other samples is low due to the small number of apertures in the lens fields. With a larger sample of lens targets, the differences in distributions may become more significant.

Somewhat surprisingly, the control samples show evidence of significant difference from each other, with 10 instances where the KS test indicates that there is less than a 1% chance that the pure-parallel and COSMOS samples are drawn from the same parent distribution. Most of these low probabilities occur for the bins where $m = 22$ or 23. Furthermore, in nearly every case, it appears that the COSMOS fields are overdense compared to the pure parallel fields (e.g., Figure 2b). While this is an unexpected result, since both the COSMOS and the pure-parallel fields were chosen to be “fair” representations of the Universe, it is perfectly possible that the contiguous COSMOS area is not large enough to escape being a biased line of sight through the Universe. In fact, our results are consistent with analyses by the COSMOS team, which find that, in the magnitude range $22 < i < 23$, the field chosen for the COSMOS observations has higher clustering amplitudes than those found in surveys of other fields (McCracken et al. 2007). Also, the COSMOS weak lensing maps (Massey et al. 2007; Leauthaud et al. 2007) show more structure than seen typical simulation fields (Faure et al. 2009). In this case the pure parallel sample, albeit small, appears to provide a better indication of expected number counts in images of this depth.

4 BAYESIAN ANALYSIS

To objectively compare the number counts in the lens and control fields, and assess whether they are consistent, we also conduct a Bayesian analysis of the number count distributions.

4.1 Poisson Fluctuations

The first effect that needs to be considered in the Bayesian analysis is that of counting statistics. That is, given an underlying expectation value, μ , for the number of galaxies in a given aperture and magnitude bin, what is the likelihood function for the observed number counts, N_i , for each field i ? This is simply the Poisson probability function

$$P(N_i|\mu) = \frac{e^{-\mu}\mu^{N_i}}{N_i!}, \quad (1)$$

where $P(N_i|\mu)$ is already normalized. In the top row of Figure 3 we show representative plots that include both the distributions of

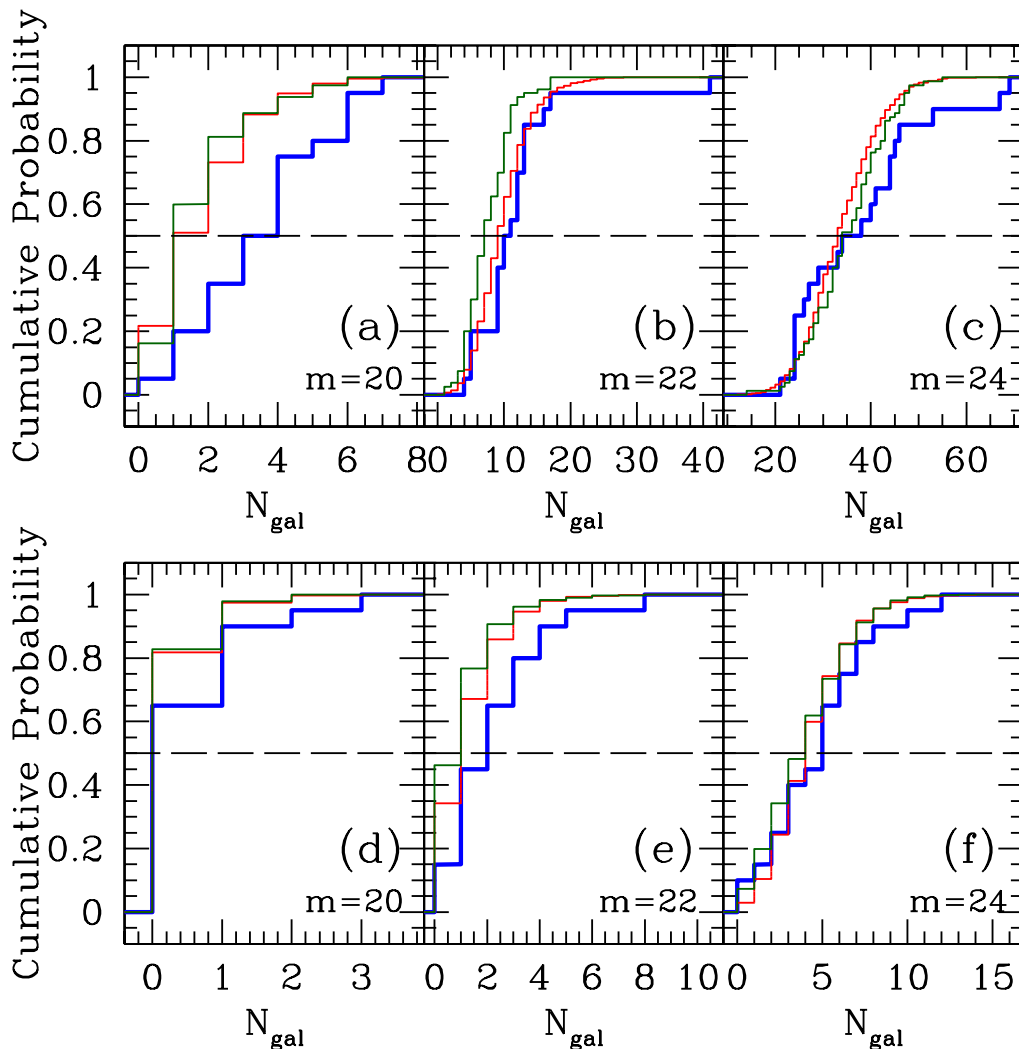


Figure 2. Cumulative distribution of number counts for six representative aperture–magnitude pairs. The magnitude bin used to construct each plot is shown in the bottom right corner of the plot. The horizontal dashed line in each plot represents a cumulative probability of 0.5 and can thus be used to find the medians of the distributions. The thick blue curves represent the lens sample. The thin curves show the COSMOS sample (red) and the pure parallel sample (green). (**Top row**) 45'' apertures. (**Bottom row**) 15''9 apertures.

the observed COSMOS number counts (histograms) and the corresponding Poisson distributions with the same means (solid curves). Figure 3a shows that the Poisson description works well for distributions with small means, in this case a bright-magnitude bin for the 45'' aperture. In contrast, as μ becomes large (e.g., Figure 3c), the observed distribution becomes wider than the predicted one, suggesting that different apertures have different underlying density fields, i.e., the same value of μ cannot be used for all apertures of a given size. Clearly the analysis requires another term.

4.2 Sample (“Cosmic”) Variance

The additional term is necessary because the presence of large-scale structure produces field-to-field variations, i.e. sample variance, in the expectation value of the underlying density field. To model this large-scale structure term, commonly described as “cosmic variance”, we assume that the field-to-field variations, for a fixed aperture, within the lens and control samples can, in each

case, be approximated as a Gaussian random field (Bardeen et al. 1986) for $\mu > 0$, i.e.

$$P(\mu|\mu_0, \sigma_0) \propto \exp\left(-\frac{(\mu - \mu_0)^2}{2\sigma_0^2}\right) \quad (2)$$

and $P(\mu|\mu_0, \sigma_0) = 0$ for $\mu \leq 0$. The integral over the probability function is properly normalized to unity. The values of μ_0 and σ_0 for a given aperture size are held fixed *within* each ensemble of fields (i.e., lens, COSMOS, or pure parallel) but can vary *between* ensembles.

Using Bayesian theory to combine the two effects gives

$$P(N_i|\mu_0, \sigma_0) = \int P(N_i|\mu)P(\mu|\mu_0, \sigma_0)d\mu, \quad (3)$$

and, combining the different fields within a given sample into a single data set $\{N_i\}$, with

$$P(\mu_0, \sigma_0|\{N_i\}) = \frac{P(\mu_0, \sigma_0) \prod_i P(N_i|\mu_0, \sigma_0)}{P(\{N_i\})}. \quad (4)$$

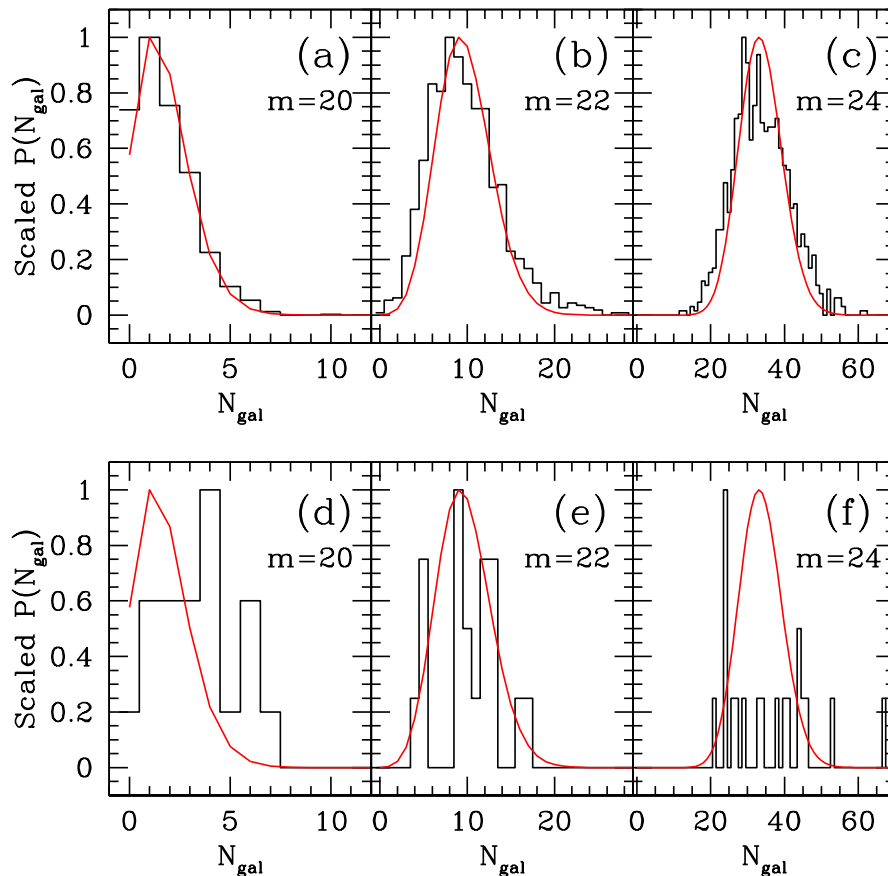


Figure 3. Histograms of number counts in the $45''$ aperture for two different samples: COSMOS (a–c) and lens fields (d–f). Shown are the magnitude bins $m = 20, 22, 24$ from right to left in each row. In both rows, the histograms represent the observed data while the solid curves represent a Poisson distribution with the same mean as the COSMOS data. Therefore, the Poisson distributions for the lens fields may not have the same means as the observed lens distributions. Whereas for bright galaxies the number-count variance can be explained by Poisson fluctuations, at fainter magnitudes (i.e. higher number counts; see panels *b* and *c*) the effect of sample variance becomes apparent.

We assume a flat prior on μ_0 , because it must be invariant under shifts, and a flat prior on $\log(\sigma_0)$, because it must be invariant under multiplication (e.g., Gregory 2005). Finally, we marginalize over σ_0 , which to us is a nuisance parameter, and get

$$P(\mu_0|\{N_i\}) = \int P(\mu_0, \sigma_0|\{N_i\}) d\sigma_0. \quad (5)$$

To obtain the median and 68% confidence contour, we construct a marginalized probability distribution from $P(\mu_0|\{N_i\})$ and find the μ_0 values corresponding to cumulative probabilities of 0.16, 0.5 (median), and 0.84. In Fig. 4, we illustrate the above process by an example for the $45''$ aperture and for $m = 22$.

4.3 Results of Bayesian Analysis

We calculate μ_0 for the lens and control fields as a function of the aperture size and magnitude. The results are shown in Figure 5 and listed in Table 3.

Figure 5 shows significant differences between the values of μ_0 obtained for the two control samples. Especially in the magnitude bins corresponding to $21 \leq m \leq 23$, the COSMOS galaxy densities are systematically higher than those seen in the pure parallel fields. This result is similar to that obtained from the KS analysis

(Table 2 and Figure 2) and also with the analysis by the COSMOS team, which finds that the amount of structure in the COSMOS field is at the high end of the range of variations produced by sample variance (McCracken et al. 2007).

It is also instructive to plot the results in terms of the offsets in μ_0 with respect to one of the samples. For this exercise, the fiducial sample is set to the pure-parallel sample because the COSMOS field appears to be biased high. Figure 6 shows the resulting offsets in μ_0 . Two trends are seen in the plot: (1) For all apertures, the COSMOS-field values of μ_0 are higher than the pure-parallel values in the range $21 \leq m \leq 23$, often at high significance, and (2) the lens fields often appear overdense compared to the pure-parallel fields, but the uncertainties on the lens values are so large that very few of the offsets are significantly different from zero. This result is consistent with our frequentist analysis of the data (§3). Clearly, a much larger lens sample is needed in order to evaluate whether the differences in number counts are real or are mostly due to statistical fluctuations in a small data set. Only for the smallest aperture ($15''$) do we see a significant trend for the lens fields, with the three bins at $m < 22$ all being $\geq 1\sigma$ higher than the pure parallel values (before the correlation function correction [§4.4]). To quantify the differences between the fields, we integrate the expect-

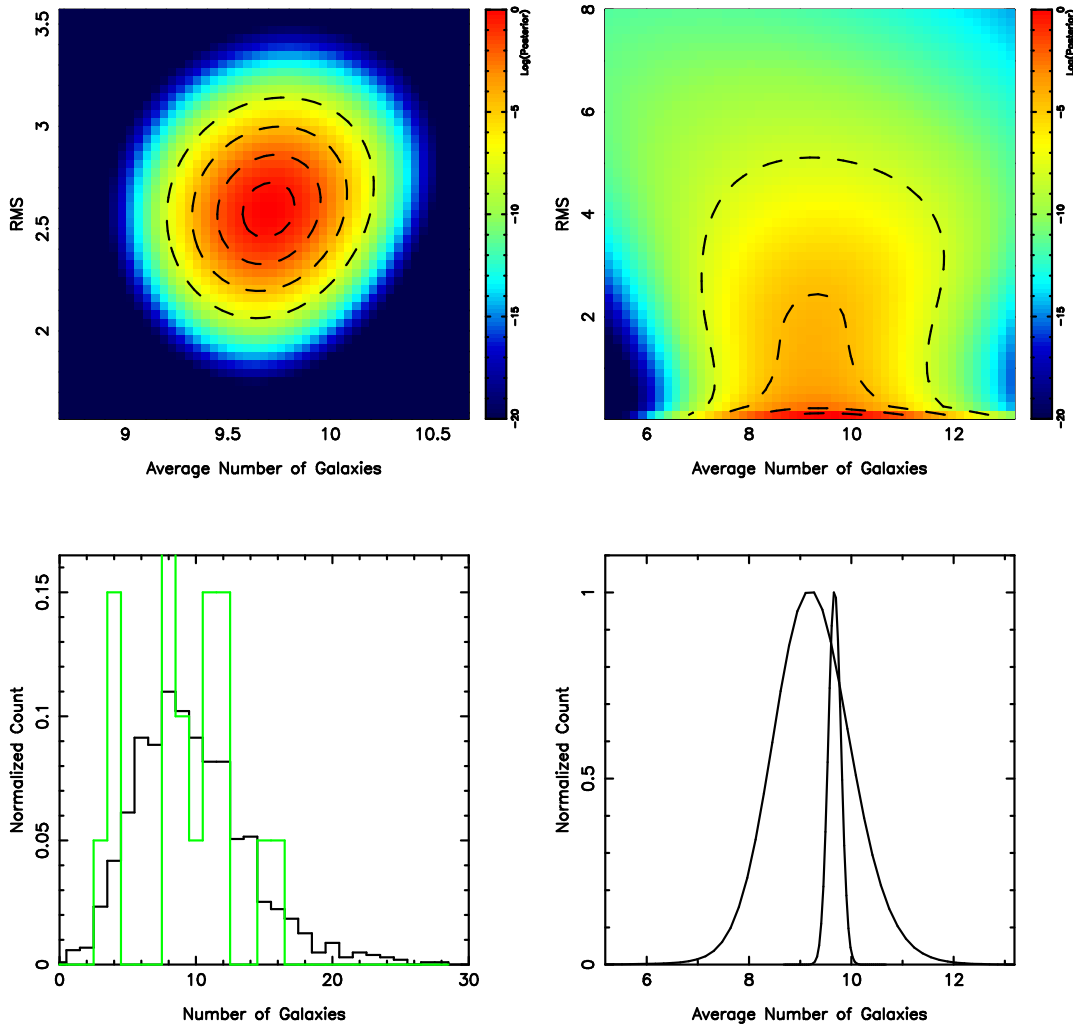


Figure 4. Bayesian inference of the mean global galaxy number density, μ_0 , for the lens and control fields. Shown is the result for the largest ($45''$) aperture and $m = 22$ magnitude bin. Shown in the lower-left panel are the (normalized) number counts of lens (green) and control fields (black; COSMOS in this case) as function of the number of galaxies in those fields. The upper two panels show the posterior probability density of (μ_0, σ_0) for the lens (right) and control (left) fields, as determined from equation 4. The lower-right panel shows the marginalized probability function of μ_0 for the lens (broad function) and control (narrow function) fields.

tation values in Table 3 over magnitude ($19 \leq m \leq 24$) to obtain the typical number of galaxies (N_{int}) in each sample. Taking $\Delta N_{\text{int}} \equiv N_{\text{int,lens}} - N_{\text{int,pp}}$, we find that $\Delta N_{\text{int}} = 6.1 \pm 3.7, 2.2 \pm 3.8, 0.7 \pm 2.8$ and 2.9 ± 1.9 galaxies for the $45'', 31'', 22''$ and $15''$ apertures, respectively. In each case, the error is dominated by the error in $N_{\text{int,lens}}$.

Overall, we can conclude that over a wide range of apertures ($\leq 45''$), the difference in the number of galaxies between lens and control fields is less than ~ 6 galaxies. Although this can be fractionally large, it clearly shows that on average only a few galaxies determine the difference between lens fields and non-lens fields in typical observations. For the smallest aperture of $15''$, the difference is typically ≤ 1 galaxy at the 68% confidence level in any given magnitude bin. However, since these galaxies are, by definition, at small projected radii from the lens, they have most influence on the lensing potential. It may be appropriate to explicitly include these galaxies in the lens model, based on an evaluation of their estimated mass and projected distance to the lens.

4.4 Correlation-function Corrections

In the previous subsection we saw that over the entire range of aperture sizes and magnitude limits, the average difference in the number of galaxies seen in the lens and control fields is typically $\lesssim 6$ for aperture sizes of $45''$, integrated over $19 \leq m \leq 24$ (e.g., Fig. 6). The slight excess seen in the lens fields is not unexpected because the massive lens galaxies typically reside in *locally* overdense regions and, in principle, one would expect more galaxies in their neighborhood.

To quantify the effect of local overdensities, we use a two-point correlation function. We assume the functional form $\omega(\theta) = A_\omega(\theta/1')^{-\delta}$ with $\delta = 0.8$ from McCracken et al. (2007). Although both our analysis and that conducted by McCracken et al. (2007) use F814W magnitudes, they use AB magnitudes while we use Vega magnitudes. Therefore, we subtract 0.42 from their

Table 3. Estimated value of the mean underlying number counts μ_0 in the lens, COSMOS, and pure-parallel fields.

Radius (Arcsec.)	m (mag.)	μ_0 (COSMOS)	μ_0 (Pure-parallel)	μ_0 (Lens)	Correlation Function Correction ($\Delta\mu_0$)	Corrected μ_0 (Lens)
45.0	19	$0.67^{+0.04}_{-0.07}$	$0.5^{+0.2}_{-0.3}$	$0.5^{+0.3}_{-0.2}$	0.15 ± 0.08	$0.4^{+0.3}_{-0.2}$
	20	1.70 ± 0.05	$1.6^{+0.2}_{-0.1}$	2.5 ± 0.5	0.22 ± 0.11	2.3 ± 0.5
	21	4.32 ± 0.08	3.5 ± 0.2	3.8 ± 0.5	0.33 ± 0.17	3.5 ± 0.5
	22	9.7 ± 0.1	7.5 ± 0.4	$9.2^{+0.8}_{-0.7}$	0.44 ± 0.22	$8.7^{+0.8}_{-0.7}$
	23	20.1 ± 0.2	17.6 ± 0.6	19.4 ± 1.7	0.56 ± 0.28	18.9 ± 1.7
	24	33.5 ± 0.2	$34.9^{+0.6}_{-0.5}$	36.4 ± 3.0	0.56 ± 0.28	35.8 ± 3.0
31.8	19	$0.32^{+0.02}_{-0.11}$	0.2 ± 0.1	$0.4^{+0.3}_{-0.2}$	0.10 ± 0.05	$0.3^{+0.3}_{-0.2}$
	20	$0.85^{+0.03}_{-0.04}$	$0.7^{+0.1}_{-0.2}$	1.0 ± 0.3	0.14 ± 0.07	0.9 ± 0.3
	21	2.14 ± 0.03	1.7 ± 0.1	$2.0^{+1.1}_{-1.3}$	0.22 ± 0.11	$1.8^{+1.1}_{-1.3}$
	22	4.90 ± 0.06	3.5 ± 0.3	$2.5^{+2.2}_{-1.7}$	0.29 ± 0.15	$2.2^{+2.2}_{-1.7}$
	23	10.10 ± 0.08	8.6 ± 0.3	$9.6^{+2.0}_{-1.9}$	0.37 ± 0.18	$9.2^{+2.0}_{-1.9}$
	24	16.64 ± 0.1	15.8 ± 0.4	$17.3^{+1.9}_{-2.0}$	0.37 ± 0.19	$16.9^{+1.9}_{-2.0}$
22.5	19	$0.04^{+0.10}_{-0.02}$	$0.11^{+0.06}_{-0.08}$	$0.4^{+0.4}_{-0.3}$	0.06 ± 0.03	$0.4^{+0.4}_{-0.3}$
	20	$0.42^{+0.01}_{-0.06}$	0.38 ± 0.04	$0.3^{+0.3}_{-0.2}$	0.09 ± 0.05	$0.2^{+0.3}_{-0.2}$
	21	1.03 ± 0.02	0.7 ± 0.1	$1.7^{+0.5}_{-0.6}$	0.14 ± 0.07	$1.5^{+0.5}_{-0.6}$
	22	2.42 ± 0.03	1.8 ± 0.1	$1.8^{+1.4}_{-1.2}$	0.19 ± 0.10	$1.6^{+1.4}_{-1.2}$
	23	5.04 ± 0.04	4.5 ± 0.2	$3.8^{+1.6}_{-1.9}$	0.24 ± 0.12	$3.6^{+1.6}_{-1.9}$
	24	8.37 ± 0.05	8.4 ± 0.2	$8.6^{+1.0}_{-1.1}$	0.24 ± 0.12	$8.4^{+1.0}_{-1.1}$
15.9	19	0.08 ± 0.01	$0.07^{+0.02}_{-0.04}$	$0.7^{+0.6}_{-0.4}$	0.04 ± 0.02	$0.6^{+0.6}_{-0.4}$
	20	0.10 ± 0.01	$0.18^{+0.02}_{-0.04}$	$0.5^{+0.4}_{-0.3}$	0.06 ± 0.03	$0.4^{+0.4}_{-0.3}$
	21	0.48 ± 0.01	$0.12^{+0.20}_{-0.07}$	0.9 ± 0.4	0.09 ± 0.05	0.8 ± 0.4
	22	1.14 ± 0.02	0.4 ± 0.1	$1.2^{+0.6}_{-0.7}$	0.13 ± 0.06	$1.0^{+0.6}_{-0.7}$
	23	2.51 ± 0.02	1.9 ± 0.1	$2.3^{+0.6}_{-1.1}$	0.16 ± 0.08	$2.1^{+0.6}_{-1.1}$
	24	4.18 ± 0.02	3.8 ± 0.1	$3.9^{+0.7}_{-1.1}$	0.16 ± 0.08	$3.8^{+0.7}_{-1.1}$

F814W AB magnitudes to obtain Vega magnitudes². It appears that, given the errors, a linear correlation between $\log(A_\omega)$ and F814W magnitude is a fairly good description of the normalization constant with $\log(A_\omega) = -1.0 \pm 0.25$ at $m = 19$ and $\log(A_\omega) = -2.1 \pm 0.1$ at $m = 24$, covering the entire observed magnitude range. We now have a functional form that allows us to determine the expected overdensities in the lens fields by integrating over $\omega(\theta)$ from 2.5 arcsec (our inner cutoff) to the aperture radius and multiplying this by the average density in the field. Although the fractional uncertainties on the normalization constants are large for the bright magnitudes, the numbers of galaxies in these bins is small. Thus, the uncertainties on the predicted number of additional galaxies will be < 1 galaxy.

In addition to the uncertainties in $\log(A_\omega)$, there is an uncertainty on the estimated number of excess galaxies that comes from the value used for the average density in the field. We have assumed that the average galaxy densities over the full COSMOS and pure-parallel field areas provide a reasonable approximation since they are either derived from a very large field or from randomly pointed fields, respectively. Even if they themselves are slightly over- or underdense on these scales, we do not expect the shape of the correlation function to be significantly altered. Thus, the effect of, say, the overdensity seen in the COSMOS field (e.g., Fig. 6) is to produce a slight overestimate on the correction ($\Delta\mu_0$). In response to this potential overcorrection we broaden the errors on $\Delta\mu_0$. Because this is a correction on a correction, however, its effect is only second-order. Given the errors on the normalization, we conservatively estimate (assuming a variation up and down by $1-\sigma$ in all

magnitude bins) an upper limit for the error on $\Delta\mu_0$ of $\sim 50\%$. We use this upper limit for the uncertainties on all subsequent estimates of the total number of additional galaxies.

To test the validity of the two-point correlation correction, we compared two sets of number counts derived from COSMOS. The first set is the one that we have used as the first control sample, with number counts computed in grids of apertures placed on each COSMOS field. This set should be considered to represent “random” lines of sight through the COSMOS fields, since there is nothing special about the location of the aperture centers. In contrast, the apertures in the second set are each centered on a bright ($m < 20.5$) galaxy found in the COSMOS area. The bright-galaxy sample contains 1801 apertures. In Figure 7, we plot (1) the COSMOS “random” number counts, (2) the bright-galaxy number counts, and (3) the sum of the “random” number counts and the two-point correlation correction. The corrected random number counts are in excellent agreement with the number counts in apertures centered on bright galaxies.

We can integrate the correlation-function corrections over magnitude ($19 \leq m \leq 24$) to estimate the total *excess* number of galaxies, $\Delta\mu_{0,\text{int}}$, that are expected in each of the aperture sizes. This calculation gives $\Delta\mu_{0,\text{int}} = 2.0 \pm 1.0$, 1.3 ± 0.7 , 0.9 ± 0.5 , and 0.6 ± 0.3 galaxies, in the $45''$, $31''.8$, $22''.5$ and $15''.9$ apertures, respectively. We subtract these values from the observed lens-field excesses to correct for clustering, and find integrated differences of $\Delta N_{\text{int,corrected}} = 4.1 \pm 3.8$, 0.9 ± 3.9 , -0.2 ± 2.8 and 2.3 ± 1.9 , respectively. In other words, after correcting for galaxy clustering, the lens and pure-parallel (or COSMOS) fields differ at less than the $2-\sigma$ level.

² The ACS zeropoints for the Vega and AB systems can be obtained at <http://www.stsci.edu/hst/acs/analysis/zeropoints>.

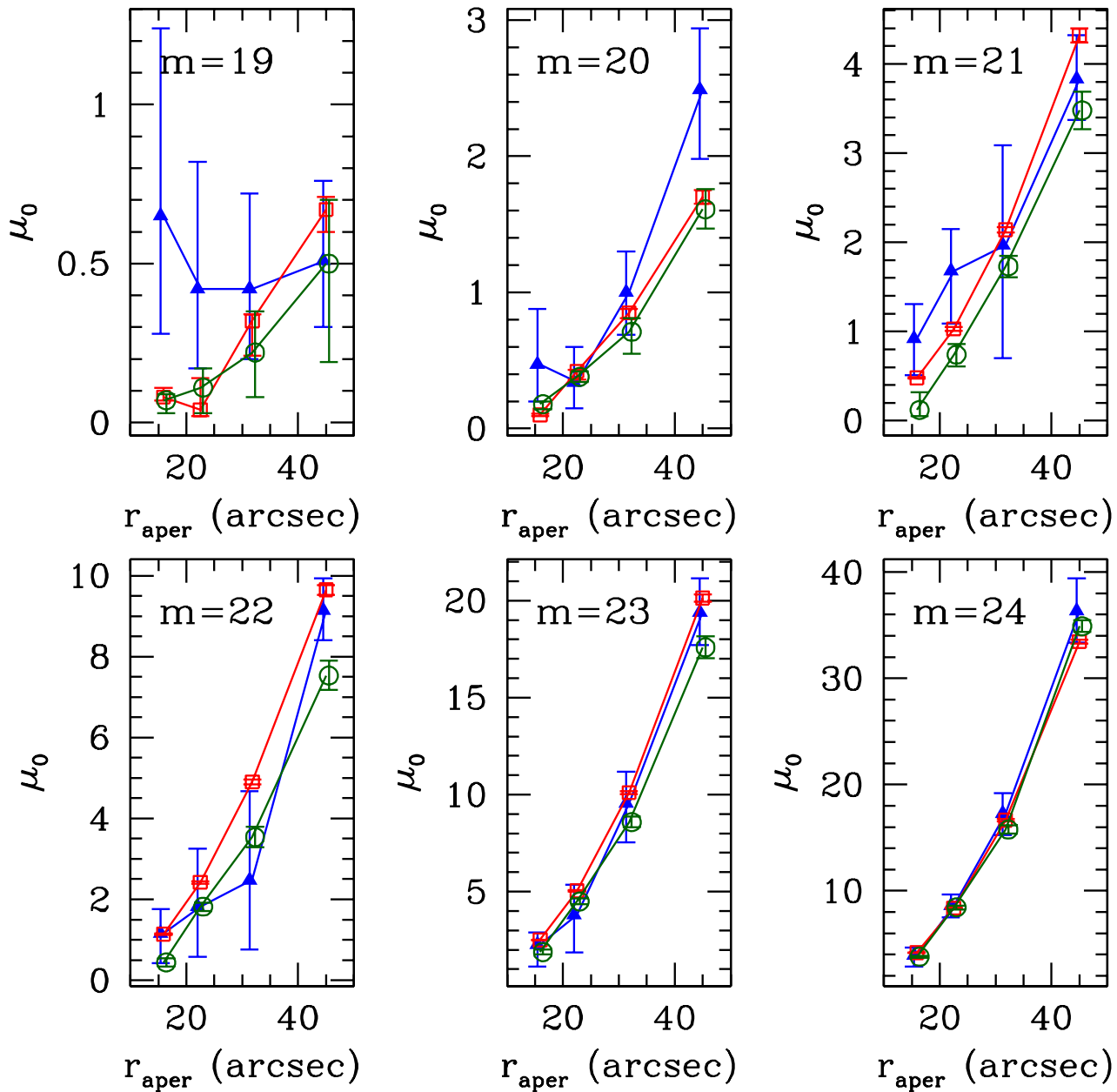


Figure 5. Plots of μ_0 vs. aperture size for each magnitude bin. In each plot, the blue triangles represent the lens sample, the red open squares represent the COSMOS sample, and the green open circles represent the pure-parallel sample. The value of μ_0 is determined for each aperture independently. Thus, for small numbers of galaxies, such as in the $m = 19$ bin, it is possible to have a larger fitted value of μ_0 in a smaller aperture than in the next larger aperture. Note that the COSMOS and pure-parallel points are formally inconsistent in several of the plots (e.g., $m=21$, 22, and 23).

5 INTERPRETATION

Drawing firm conclusions from our Bayesian analysis is hampered by the small number of lens fields in our sample. There can be two interpretations of our results: (1) that any line-of-sight overdensities in the lens fields are insignificant once the local overdensities around the lens galaxies are accounted for, and will remain insignificant even with a large increase in the size of the lens-field sample, or (2) the overdensities we see in $N_{\text{int,corrected}}$ for, e.g., the $45''$ and $15''.9$ apertures will become significant once more lens fields

can be included in the analysis and the errors on the estimates of $\mu_{0,\text{lens}}$ shrink. Distinguishing between the two will clearly need a larger lens sample. However, it should be noted that even if a future larger lens sample indicates that the differences between the lens and control fields are significant, the excess number of galaxies in the lens fields is only, on average, $\Delta\mu_{0,\text{int}} \lesssim 4$ for average integrated number counts of $N_{\text{int}} \sim 70$; i.e., $\sim 6\%$.

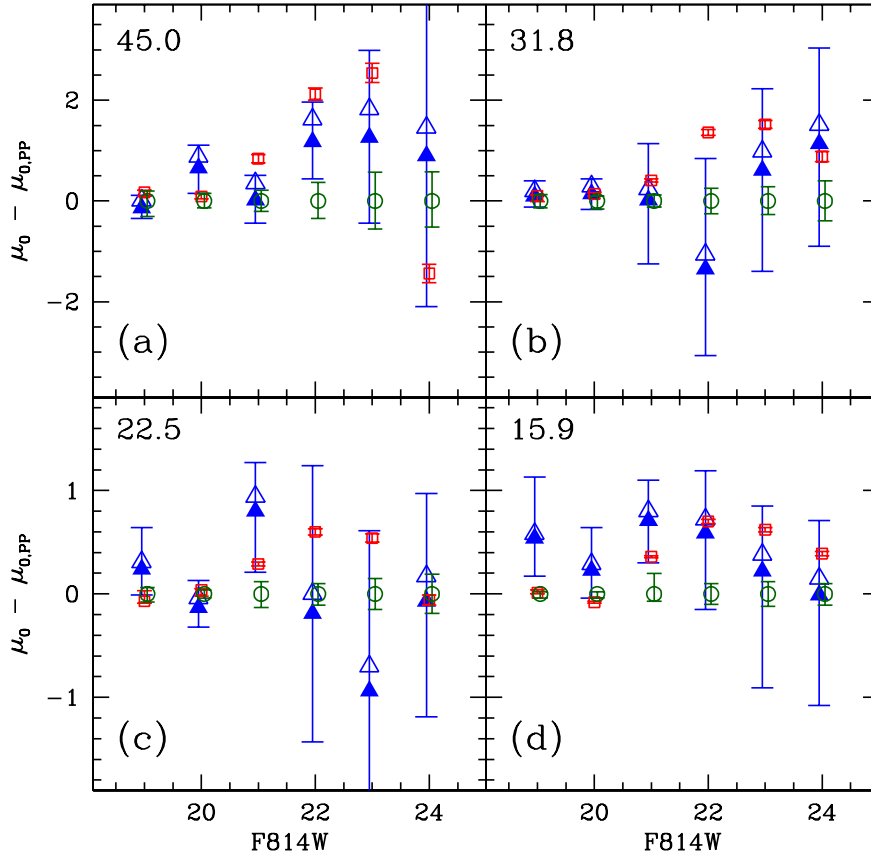


Figure 6. Results of Bayesian analysis, showing the *difference* between the values of μ_0 calculated for lens (blue triangles) and COSMOS fields (red squares) and those obtained for the pure parallel fields (green circles). The open blue triangles represent the lens-field values *before* correcting for clustering of massive galaxies, while the solid blue triangles represent the lens-field values *after* the correction has been applied (see §4.4). Note the highly significant displacement between the pure parallel fields and the COSMOS fields, particularly for $21 \leq m \leq 23$.

5.1 Comments on Individual Lens Systems

Of course, the average values that have been determined in the preceding sections can hide a large variation from lens system to lens system. Fig. 8 shows the difference between the cumulative number counts of the lens sample and the pure-parallel mean cumulative counts (ΔN_{int}) for the $45''$ aperture. For the bright galaxies ($m \leq 22$), the lens fields with the largest overdensities are, in order starting with the most overdense, SDSS J1004+4112, B1608+656, and B2108+213. If considering all galaxies with $m \leq 24$, the three most overdense fields are SDSS J1004+4112, B1608+656, and B0218+357 (the three highest in Fig. 9). All of these fields are outside the region enclosing 90% of the COSMOS data. The overdensities for SDSS J1004+4112 and B2108+213 are not particularly surprising because both of these systems are known to be associated with a cluster or rich group (Oguri et al. 2004; McKean et al. 2010). However, neither B1608+656 nor B0218+357 appear to be physically associated with such massive concentrations of galaxies. Spectroscopic observations of the B1608+656 field have revealed multiple group-sized associations along the line of sight (Fassnacht et al. 2006b), but the B0218+357 field will have to be

examined more closely in future analyses. Fig. 8 also reveals fields that are underdense with respect to the mean. The most underdense in bright galaxies are SDSS 1226–0006, J0816+5003, and B0850+054.

The distributions of integrated lens number counts shown in Figures 8 and 9 reveal some interesting points. One is that there are significant more high outliers in the lens distribution than would be expected given the control-field distributions. This effect is almost certainly due in part to small number statistics, and the highest point in the integrated number count distribution in Fig. 9 is due to an obvious cluster lens. However, the next two highest points in that distribution are due to galaxy-scale lenses that were selected in a radio survey targeting the background objects (Browne et al. 2003). Because these lens systems were discovered in a source-selected survey, they should not be biased toward high number counts in the way that surveys targeting the likely lensing galaxies (i.e., massive ellipticals) could be. The second point, somewhat related, is that our Bayesian analysis has produced clearly different estimates of the “typical” number counts than other measures such as the sample mean or median for the lens sample (Fig. 8). This is in contrast to the behaviour in the control fields, where the sample means are ex-

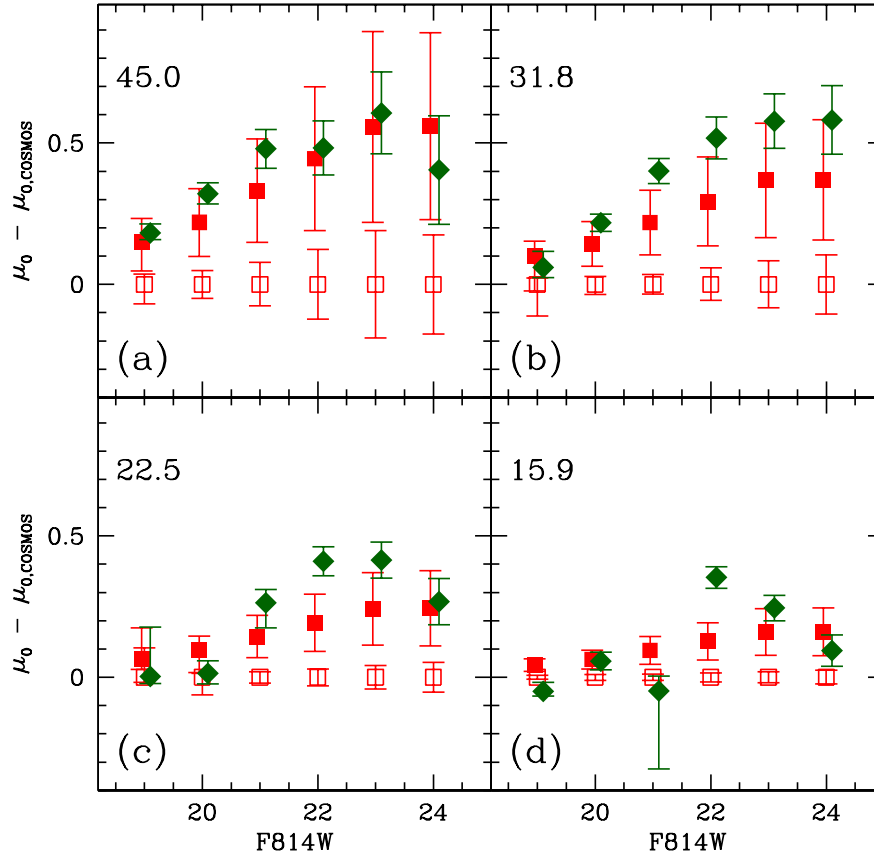


Figure 7. Comparison of number counts between the COSMOS control sample (open red squares) and apertures centered on bright galaxies in COSMOS (green diamonds). The filled red squares represent the sum of the control sample number counts and the two-point correlation correction factors.

cellent matches to the calculated values of N_{int} . Clearly the mean of the lens sample is pulled high by the outliers, but the median should be a more robust estimator. A significantly larger lens sample is needed to assess whether these behaviours are due to small-number statistics or are indicative of a slight bias in the lens-field counts.

5.2 Implications for H_0

Because B0218+357 (Biggs et al. 1999), SDSS J1004+4112 (Fohlmeister et al. 2007, 2008), and B1608+656 (Fassnacht et al. 1999, 2002) are systems for which time delays have been measured, the galaxy overdensities must be included in any analysis to determine H_0 from these systems. The over- and underdensities in mass along the line of sight to a lens system, quantified by the external convergence (κ_{ext}), bias the determination of H_0 from that system if not taken properly into account. The correct value of H_0 from a given field is $H_0 = (1 - \kappa_{\text{ext}})H_{0,\text{uniform}}$, where $H_{0,\text{uniform}}$ is the value of H_0 obtained without taking into account the external convergence. In theory, it should be possible to use our number-count approach to obtain an estimate of κ_{ext} for a given lens. The problem, of course, is how to convert the observed galaxy numbers into an accurate mass measurement.

One approach to estimate κ_{ext} has been presented by Suyu et al. (2010), in which they estimate a probability density function for κ_{ext} using a method similar to that used in Hilbert et al. (2007). In particular, they trace rays through the Millennium Simulation (Springel et al. 2005), and determine the distributions of κ_{ext} between the redshift of the background source and the observer. However, rather than examining the full distribution of κ_{ext} obtained from all lines of sight, the κ_{ext} distribution is estimated using only those lines of sight that have fractional galaxy number count overdensities matching those observed in the field of the real lens. The Suyu et al. (2010) analysis used our results for the fractional overdensity along the B1608+656 line of sight (~ 2 compared to the pure parallel sample) to obtain the prior on κ_{ext} . To aid in similar analyses of time delay lens systems, we have provided in Table 4 the integrated number counts and fractional over/underdensities with respect to the pure parallel sample for each of the lens systems considered here.

In order to explore the effects that line-of-sight variations in N_{int} may have on future attempts to determine a global value of H_0 , we have undertaken a simple simulation. This simulation relies on four major assumptions, at least three of which are questionable; the point of this exercise is solely to explore in a very rough sense the possible implications of the number counts mea-

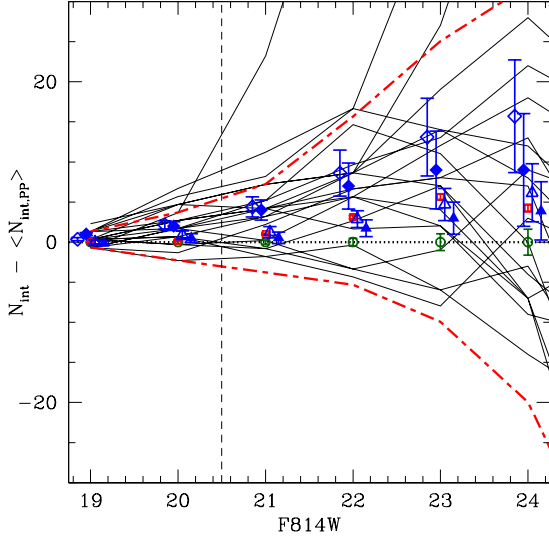


Figure 8. Offsets between the cumulative number counts calculated in individual lens fields (light lines) and the pure-parallel mean cumulative number counts (green circles) in apertures of radius $45''$. The blue points represent four ways of representing the lens-field distribution: the mean (open diamonds), the median (filled diamonds), $\mu_{0,\text{int}}$ from the Bayesian analysis (open triangles), and the corrected $\mu_{0,\text{int}}$ (filled triangles). The blue points have been offset slightly in the horizontal direction for clarity. The COSMOS distribution is also shown by its mean (red squares), and 90% range (red dot-dashed lines). The light dashed vertical line is placed solely to identify the three most overdense lens fields. Starting at the top of the figure and going down, the line encounters, in order, the curves for SDSS J1004+4112, B1608+656, and B2108+213, all of which fall outside the 90% range of COSMOS field number counts.

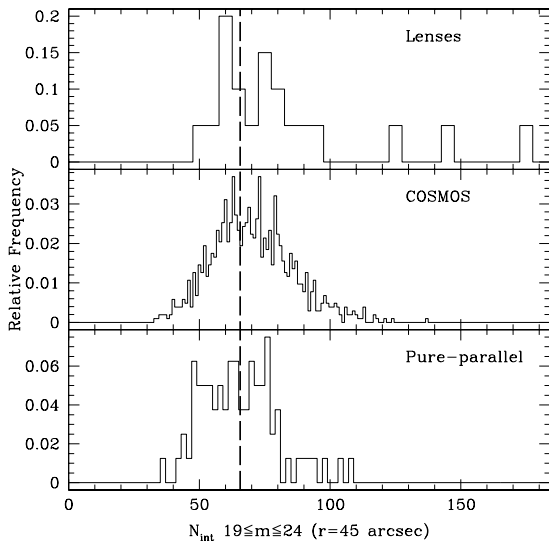


Figure 9. Distribution of the integrated number counts for all galaxies with $m \leq 24$ inside $45''$ apertures, for each of the three samples. The vertical dashed line represents the mean of the pure-parallel sample.

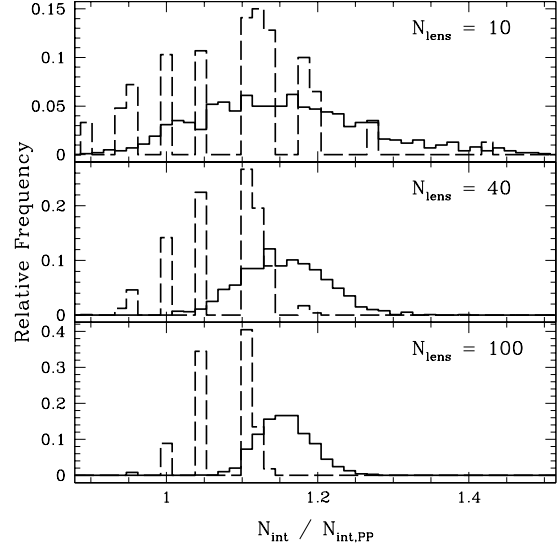


Figure 10. Distributions of the sample means (solid curves) and medians (dashed curves) of the integrated number counts obtained in simulated lens-field samples. In each case, 1000 realizations were obtained. The three panels show sample sizes of $N_{\text{lens}} = 10, 40, \text{ and } 100$.

sured in this paper. The first assumption is that true distribution of integrated number counts in lens fields is given by the top panel of Fig. 9. Given our small sample of only 20 lens systems, this assumption is almost certainly in error. We do eliminate the field with the highest integrated number counts since that is associated with a clear cluster-scale lens and is not representative of the galaxy-scale lenses in the other 19 fields. The second assumption is that the true mean integrated number counts are given by the values obtained from our analysis of the pure-parallel sample. The third assumption is that the overall determination of H_0 from the lens sample is made without any correction for variations in κ_{ext} from field to field. The fourth assumption is discussed below.

The first step in the simulation is to create 1000 realizations of a sample of N_{lens} lenses via a bootstrap procedure, i.e., by drawing N_{lens} values of N_{int} randomly, but with replacement, from the distribution shown in the top panel of Fig. 9. We consider three cases, $N_{\text{lens}} = 10, 40, \text{ and } 100$. For each realization we calculate the mean and median of the N_{int} distribution, and divide by $N_{\text{int,PP}}$ to facilitate our later estimates of κ_{ext} . The resulting distributions are shown in Fig. 10. The widths of the distributions of mean values shows the expected $1/\sqrt{N}$ behaviour, with the sample RMS values being 0.11, 0.055, and 0.033 for $N_{\text{lens}} = 10, 40, \text{ and } 100$, respectively. However, our assumption that the true lens-field distribution of N_{int} is represented by the observed distribution given in Table 4 and shown in Fig. 9 introduces a bias into the lens field counts. The centers of the distributions occur at $N_{\text{int}}/N_{\text{int,PP}}$ of 1.16, 1.15, and 1.16 for the means and at 1.09, 1.08, and 1.08 for the medians. Thus the number counts in the simulated lens samples are biased high compared to the pure-parallel sample by $\sim 15\%$ if a straight mean is taken, and by $\sim 8\%$ if a median is taken, if no attempt is made to correct for excess number counts in the lens fields.

The final step in the simulation is to convert the distributions of $N_{\text{int}}/N_{\text{int,PP}}$ into distributions of κ_{ext} . This step involves the highly questionable final assumption, namely that a simple conversion between $N_{\text{int}}/N_{\text{int,PP}}$ and κ_{ext} can be derived from the analysis of B1608+656 by Suyu et al. (2010). Their careful ray

tracing through the Millennium Simulation found that fields with $N_{\text{int}}/N_{\text{int,PP}} \sim 2$, corresponding to the case for B1608+656, produced a distribution of κ_{ext} that was roughly centered at $\kappa_{\text{ext}} \sim 0.1$. One could assume that this scaling held for all fields, and that $N_{\text{int,PP}}$ corresponded to $\kappa_{\text{ext}} \sim 0$. Under these assumptions, the bias in the lens-field integrated number counts of $N_{\text{int}}/N_{\text{int,PP}} \sim 1.15$ would correspond to $\kappa_{\text{ext}} \sim 0.02$, and the resulting global determination of H_0 from the lens sample would be biased high by $\sim 2\%$.

However, the results of the simulation are based on the assumption that no correction has been made for the estimated κ_{ext} in each lens field before averaging to obtain the global value of H_0 . A lens for which a time delay has been measured (a crucial component in determining H_0 from a lens system) will have been imaged many times as part of a monitoring campaign. Thus, the integrated number counts in each of the lens fields should be known. Therefore, it should be possible to reduce any bias due to improper accounting for κ_{ext} in lens-based determinations of the global value of H_0 if the following steps can be taken for each lens in the sample. (1) Quantitative estimates of the effect of the local environment of the lens should be made. These can come from measurements of the velocity dispersion of the lensing galaxy (e.g., Suyu et al. 2010), as well as photometric and/or spectroscopic searches for a group or cluster that is physically associated with the lensing galaxy. (2) The galaxy number counts for the lens field should be calculated within a reasonable aperture and to a reasonable magnitude limit. For the B1608+656 analysis, Suyu et al. (2010) used the integrated counts ($19 \leq m \leq 24$) within an aperture of radius $45''$. The magnitude limit should be at or brighter than the completeness limit and should sample, as much as possible, the full line of sight to the redshift of the background object. (3) Number counts with the same aperture and magnitude limits should be computed for a control sample that is expected to be representative of random lines of sight through the Universe. For the B1608+656 analysis, Suyu et al. (2010) used the pure-parallel sample rather than the COSMOS sample, since the COSMOS number counts come from a contiguous area on the sky that is not large enough to overcome sample variance. (4) After computing the ratio of the lens-field number counts to the mean of the control sample counts, the distribution of κ_{ext} can be estimated by ray tracing through a structure formation simulation, such as the Millennium Simulation (Springel et al. 2005). Details on how this was done for the B1608+656 field are given in Suyu et al. (2010). (5) This κ_{ext} distribution should be used as a prior probability in the full H_0 analysis for the lens system.

6 CONCLUSIONS

To assess whether strong gravitational lenses are preferentially found along overdense lines of sight, we have devised a straightforward Bayesian statistical number-count test which is conservative and robust. It requires only the number counts of galaxies as function of magnitude inside apertures of different sizes centered on the lenses and on control fields. We have applied this method to a sample of 20 lenses with F814W ACS images and control samples from the COSMOS and pure-parallel programs.

Our hypothesis is that if gravitational lenses are found along highly overdense lines of sight compared to random pointings on the sky, either due to structure along the line of sight or overdensities associated with the lens galaxies themselves, then the number of galaxies within apertures centered on the lenses should show on

Table 4. Integrated number counts for all galaxies with $m \leq 24$ within $45''$ apertures.

Field	N_{int}	$[N_{\text{int}}/N_{\text{int,PP}}]$
PP Mean	66	1.00
COSMOS Mean	70	1.06
JVAS B0218+357	125	1.89
CLASS B0445+128	62	0.94
CLASS B0850+054	75	1.14
CLASS B1608+656	144	2.18
CLASS B2108+213	74	1.12
CFRS 03.1077	52	0.79
HE 0435-1223	59	0.89
HE 1113-0641	59	0.89
J0743+1553	73	1.11
J0816+5003	63	0.95
J1004+1229	84	1.27
RX J1131-1231	94	1.42
SDSS 0246-0825	57	0.86
SDSS 0903+5028	59	0.89
SDSS 0924+0219	79	1.20
SDSS 1004+4112	174	2.64
SDSS 1138+0314	78	1.18
SDSS 1155+6346	66	1.00
SDSS 1226-0006	69	1.05
WFI 2033-4723	88	1.33

average more galaxies than similar apertures in the control fields. This approach is conservative in that it does not require redshifts for the galaxies (for a given magnitude, galaxies over a wide redshift range contribute to the number counts), but only that the ratio between mass and light integrated over the redshift cone is close to constant. Thus, the number of galaxies can be used as a proxy for mass; more galaxies on average implies more mass along the line of sight.

More precise statistics can be constructed if the redshifts, galaxy types, etc. are known, and the galaxy masses are derived through scaling relations such as the Tully-Fisher relation (Tully & Fisher 1977) or the fundamental plane (Djorgovski & Davis 1987; Dressler et al. 1987). However, the results of such models quickly become model-dependent and prone to systematic errors. Thus, although such approaches may show a more significant result than ours, a rejection of the hypothesis by our approach has the advantage of being a robust result that is less dependent on model assumptions.

Having applied our number-count comparison to the selected lens and control fields we find the following results:

(i) All distribution functions of number counts in the lens and control fields are well described by a combination of a Gaussian random field for the sample variance (i.e., the underlying density field varies from field to field) and Poisson statistics in the number counts. This defines our underlying Bayesian statistical model.

(ii) In the three largest apertures, with radii of $45''$, $38''$ and $22''.5$ (steps of 2 in area), we find *no* significant difference in the number counts in the individual magnitude bins between the lens and control fields (Fig. 6 and Table 3). We emphasize that this does not presuppose that there is no overdensity, just that our robust statistics do not require it. We also note that the uncertainties on the lens number counts are large, since there are only 20 lenses in our sample.

(iii) The smallest aperture ($15''.9$) centered on the lenses, however, does show significantly more galaxies in the magnitude range

$19 \leq m \leq 21$ than either the COSMOS or pure parallel fields. This is not unexpected since massive lens galaxies live in overdense regions (their two-point correlation is strong).

(iv) When we correct for the effect of the two-point correlation, using the results from COSMOS by McCracken et al. (2007), we find that a significant part of the differences between number counts in the lens and COSMOS fields can be accounted for by the fact that massive lens galaxies live in *locally* overdense regions, as expected. The remaining differences are at the $\lesssim 1-\sigma$ level in the individual magnitude bins.

(v) Even though the differences are at the $\sim 1-\sigma$ level for individual magnitude bins, the lens-field counts are consistently higher than the pure-parallel counts across several magnitude bins for the smallest and largest apertures. This behaviour may indicate real overdensities, although once again the differences in the integrated number counts are only at the $\sim 1-2-\sigma$ level. These differences could either be due to small overdensities along the line of sight (e.g., Fassnacht & Lubin 2002; Momcheva et al. 2006; Fassnacht et al. 2006b; Auger et al. 2007), or due to a too simplistic correction of the number counts for the COSMOS two-point correlation function.

(vi) On average, the excess numbers of galaxies along the lines of sight to the lensing galaxies, integrated over the magnitude range that we have explored in this paper, are small once the correlation function corrections have been applied (e.g., $\lesssim 4$ galaxies for the largest aperture that we examined). These excesses, which are mainly due to local overdensities associated with the lensing galaxy, amount to only $\sim 4-8\%$ of the total number counts in the three largest apertures. These fractional overdensities can be compared with similar numbers derived from numerical simulations. In particular, Hilbert et al. (2007) found, by ray tracing through the Millennium Simulation (Springel et al. 2005), that lenses do along biased lines of sight. The contribution of the additional mass, however, was only a few percent of the total surface mass density along those lines of sight, in good agreement with our results.

(vii) While the average number counts in our sample of 20 strong lenses does agree well with the control samples, once the effect of local clustering has been taken out, individual lens systems can still have significantly discrepant number counts. Thus, care should be taken when using an individual lens system to measure H_0 . We present a recipe for using number counts and other information to improve the treatment of line-of-sight convergence to measurements of H_0 using lenses.

Based on our statistical test, we can say that: Yes, lens galaxies do lie along overdense lines of sight compared to random pointings on the sky, but these overdensities can be at least partially explained by the fact that these massive lens galaxies are formed in locally overdense regions. We conclude that in strong-gravitational lens modeling one always needs to assess the effect of the *local* distribution of galaxies. Our test indicates that the contribution by everything else along the line of sight does not appear to be significant on average. However, a larger sample of lenses is needed to strengthen any conclusions about the significance of differences between the lens and control fields. If the possible slight excess in the lens field number counts persists in larger samples, then global determinations of H_0 using lens samples may be biased unless the analysis properly accounts for both the local overdensities and the external convergence of the fields in which the lenses are embedded.

We thank Phil Marshall, Tommaso Treu, and Maruša Bradač for fruitful discussions, and Phil for further insightful comments as

the referee of this paper. We thank Phil Marshall and Tim Schrabback for their work on the HAGGLEs pipeline and their help in modifying the pipeline to run on the pure-parallel data. CDF acknowledges support under HST program #AR-10300, which was provided by NASA through a grant from the Space Telescope Science Institute, which is operated by the Association of Universities for Research in Astronomy, Inc., under NASA contract NAS 5-26555. He is also grateful for the generous hospitality shown by the Kapteyn Institute on his visits there. LVEK is supported (in part) through an NWO-VIDI program subsidy (project number 639.042.505). This work is supported by the European Community's Sixth Framework Marie Curie Research Training Network Programme, Contract No. MRTN-CT-2004-505183 'ANGLES'.

REFERENCES

- Argo M. K., et al., 2003, MNRAS, 338, 957
 Auger M. W., Fassnacht C. D., Wong K. C., Thompson D., Matthews K., Soifer B. T., 2008, ApJ, 673, 778
 Auger M. W., 2008, MNRAS, 383, L40
 Auger M. W., Fassnacht C. D., Abrahamse A. L., Lubin L. M., Squires G. K., 2007, AJ, 134, 668
 Bardeen, J. M., Bond, J. R., Kaiser, N., & Szalay, A. S. 1986, ApJ, 304, 15
 Bar-Kana, R. 1996, ApJ, 468, 17
 Bertin, E. & Arnouts, S. 1996, A&A, 117, 393
 Biggs A. D., et al., 2003, MNRAS, 338, 1084
 Biggs A. D., Browne I. W. A., Helbig P., Koopmans L. V. E., Wilkinson P. N., Perley R. A., 1999, MNRAS, 304, 349
 Blackburne J. A., Wisotzki L., Schechter P. L., 2008, AJ, 135, 374
 Bolton A. S., Burles S., Koopmans L. V. E., Treu T., Moustakas L. A., 2006, ApJ, 638, 703
 Bolton A. S., Burles S., Koopmans L. V. E., Treu T., Gavazzi R., Moustakas L. A., Wayth R., Schlegel D. J., 2008, ApJ, 682, 964
 Browne I. W. A., Patnaik A. R., Walsh D., Wilkinson P. N., 1993, MNRAS, 263, L32
 Browne I. W. A., et al., 2003, MNRAS, 341, 13
 Crampton D., Schade D., Hammer F., Matzkin A., Lilly S. J., Le Fèvre O., 2002, ApJ, 570, 86
 Djorgovski S., Davis M., 1987, ApJ, 313, 59
 Dressler A., 1980, ApJ, 236, 351
 Dressler A., Lynden-Bell D., Burstein D., Davies R. L., Faber S. M., Terlevich R., Wegner G., 1987, ApJ, 313, 42
 Eigenbrod A., Courbin F., Dye S., Meylan G., Sluse D., Vuissoz C., Magain P., 2006, A&A, 451, 747
 Eigenbrod A., Courbin F., Meylan G., Vuissoz C., Magain P., 2006, A&A, 451, 759
 Eigenbrod A., Courbin F., Meylan G., 2007, A&A, 465, 51
 Fassnacht, C. D. & Lubin, L. M. 2002, AJ, 123, 627
 Fassnacht C. D., Pearson T. J., Readhead A. C. S., Browne I. W. A., Koopmans L. V. E., Myers S. T., Wilkinson P. N., 1999, ApJ, 527, 498
 Fassnacht C. D., Xanthopoulos E., Koopmans L. V. E., Rusin D., 2002, ApJ, 581, 823
 Fassnacht C. D., et al., 2006, ApJ, 651, 667
 Fassnacht C. D., Gal R. R., Lubin L. M., McKean J. P., Squires G. K., Readhead A. C. S., 2006, ApJ, 642, 30
 Faure C., Alloin D., Kneib J. P., Courbin F., 2004, A&A, 428, 741
 Faure C., et al., 2009, ApJ, 695, 1233
 Fohlmeister J., et al., 2007, ApJ, 662, 62

- Fohlmeister J., Kochanek C. S., Falco E. E., Morgan C. W., Wambsganss J., 2008, *ApJ*, 676, 761
- Ford, H., et al. 1998, *Proc. SPIE*, 3356, 234
- Ford, H., et al. 2003, *Proc. SPIE*, 4854, 81
- Gregory, P. C. 2005, *Bayesian Logical Data Analysis for the Physical Sciences: A Comparative Approach with 'Mathematica' Support*. Edited by P. C. Gregory. ISBN 0 521 84150 X Published by Cambridge University Press, Cambridge, UK, 2005
- Haarsma D. B., et al., 2005, *AJ*, 130, 1977
- Hilbert S., White S. D. M., Hartlap J., Schneider P., 2007, *MNRAS*, 382, 121
- Hilbert S., White S. D. M., Hartlap J., Schneider P., 2008, *MNRAS*, 386, 1845
- Inada N., et al., 2003, *AJ*, 126, 666
- Inada N., et al., 2003, *Nature*, 426, 810
- Inada N., et al., 2005, *AJ*, 130, 1967
- Johnston D. E., et al., 2003, *AJ*, 126, 2281
- Koekemoer, A. M., Fruchter, A. S., Hook, R., & Hack, W. 2002, in *2002 HST Calibration Workshop*, eds. S. Arribas, A. Koekemoer, & B. Whitmore. Baltimore, MD: Space Telescope Science Institute, 2002., p.339
- Koekemoer, A. M., et al. 2007, *ApJS*, 172, 196
- Kundić T., Cohen J. G., Blandford R. D., Lubin L. M., 1997, *AJ*, 114, 507
- Kundić T., Hogg D. W., Blandford R. D., Cohen J. G., Lubin L. M., Larkin J. E., 1997, *AJ*, 114, 2276
- Lacy M., Gregg M., Becker R. H., White R. L., Glikman E., Helfand D., Winn J. N., 2002, *AJ*, 123, 2925
- Leauthaud A., et al., 2007, *ApJS*, 172, 219
- Lehár J., Buchalter A., McMahon R. G., Kochanek C. S., Muxlow T. W. B., 2001, *ApJ*, 547, 60
- Massey R., et al., 2007, *ApJS*, 172, 239
- McCracken, H. J., et al., 2007, *ApJS*, 172, 314
- McKean J. P., Koopmans L. V. E., Browne I. W. A., Fassnacht C. D., Blandford R. D., Lubin L. M., Readhead A. C. S., 2004, *MNRAS*, 350, 167
- McKean J. P., et al., 2005, *MNRAS*, 356, 1009
- McKean J. P., et al., 2010, *MNRAS*, 404, 749
- Momcheva I., Williams K., Keeton C., Zabludoff A., 2006, *ApJ*, 641, 169
- Morgan N. D., Caldwell J. A. R., Schechter P. L., Dressler A., Egami E., Rix H.-W., 2004, *AJ*, 127, 2617
- Morgan N. D., Kochanek C. S., Pevunova O., Schechter P. L., 2005, *AJ*, 129, 2531
- Myers S. T., et al., 1995, *ApJ*, 447, L5
- Oguri M., et al., 2004, *ApJ*, 605, 78
- Patnaik A. R., Browne I. W. A., King L. J., Muxlow T. W. B., Walsh D., Wilkinson P. N., 1993, *MNRAS*, 261, 435
- Pindor B., et al., 2004, *AJ*, 127, 1318
- Schneider P., Kochanek C. S., Wambsganss J., 2006, *Gravitational Lensing: Strong, Weak and Micro: Saas-Fee Advanced Courses*, Volume 33. Springer-Verlag, Berlin, Heidelberg
- Scoville, N., et al. 2007, *ApJS*, 172, 1
- Scoville, N., et al. 2007, *ApJS*, 172, 38
- Seljak, U. 1994, *ApJ*, 436, 509
- Sluse D., et al., 2003, *A&A*, 406, L43
- Springel V., et al., 2005, *Nature*, 435, 629
- Suyu S. H., Marshall P. J., Auger M. W., Hilbert S., Blandford R. D., Koopmans L. V. E., Fassnacht C. D., Treu T., 2010, *ApJ*, 711, 201
- Treu T., Gavazzi R., Gorecki A., Marshall P. J., Koopmans L. V. E., Bolton A. S., Moustakas L. A., Burles S., 2009, *ApJ*, 690, 670
- Tully R. B., Fisher J. R., 1977, *A&A*, 54, 661
- Wambsganss J., Bode P., Ostriker J. P., 2005, *ApJ*, 635, L1
- Williams K. A., Momcheva I., Keeton C. R., Zabludoff A. I., Lehár J., 2006, *ApJ*, 646, 85
- Wisotzki L., Schechter P. L., Bradt H. V., Heinmüller J., Reimers D., 2002, *A&A*, 395, 17
- Zabludoff A. I., Mulchaey J. S., 1998, *ApJ*, 496, 39